IJSRM
INTERNATIONAL JOURNAL OF SCIENCE AND RESEARCH METHODOLOGY
An Official Publication of Human Journals

Human Journals
Research Article
January 2019 Vol.:11, Issue:3

Adsorption of Iron (II) on Sodic Zeolites—Bearing Brick (In Batch): Insights into Interfacial Chemical Processes and Thermodynamic Equilibria

IJSRM
INTERNATIONAL JOURNAL OF SCIENCE AND RESEARCH METHODOLOGY
An Official Publication of Human Journals

Nicole Poumaye[1,2], Oscar Allahdin[1,2], Ludovic Lesven[2], Michel Wartel[2], Abdel Boughriet[2*]

1. Chaire Unesco « Sur la gestion de l'eau », Laboratoire Hydrosciences Lavoisier, Université de Bangui, Faculté des Sciences, B.P. 908, République Centrafricaine.

2. Université Lille, Laboratoire LASIR (UMR CNRS 8516), Equipe Physico-chimie de l'Environnement. Bât. C8 2ème étage, 59655 Villeneuve d'Ascq cedex, France.

Submission: 25 December 2018
Accepted: 31 December 2018
Published: 30 January 2019

Keywords: Zeolites; iron(II); adsorption isotherms; interfacial equilibria; thermodynamics.

ABSTRACT

Zeolitization of a brick containing metakaolinite was carried out under varying alkaline conditions. XRD analysis revealed the formation of crystalline structures identified as NaA and NaP zeolites. ESEM/EDS analysis confirmed the existence of cubic (NaA) and spherical (NaP) crystals at the brick surface. From batch experiments, the adsorption of iron (II) on to these synthesized brick compounds was examined at different temperatures from 293K to 308K. Iron (II) adsorption data obtained were described by considering the following isotherm models: Freundlich; Langmuir; and Dubinin-Radushkevich. Chemical (batch) data and ^{1}H and ^{23}Na MAS NMR analyses allowed us to prove the occurrence of an ion-exchange reaction between hydrated sodium (bound to brick surfaces) and Fe^{2+} ions (in the liquid phase) at the brick-water interface. To better understand the adsorptive mechanism involved in our system, comparative thermodynamic studies were made by utilizing the two dimensionless equilibrium constants: distribution and partition coefficients. Thermodynamic parameters calculated (with no significant difference) from these two methods indicated that the process occurred spontaneously ($-\Delta G°$), in an endothermic nature ($+\Delta H°$), and with increased randomness ($+\Delta S°$).

HUMAN JOURNALS
www.ijsrm.humanjournals.com

INTRODUCTION:

Nowadays, ground waters are used by many people as drinking water. But, these water sources are often contaminated with iron that is usually in its oxidation state +2, and mainly in the dissolved forms: Fe^{2+} and/or $Fe(OH)^{+}$. The maximum level of dissolved iron in drinking water which is recommended by The World Health Organization is 0.3 $mg.L^{-1}$ [1]. After lifting ground waters towards the surface, iron(II) is oxidized progressively by atmospheric oxygen to give colloidal iron oxide/hydroxide. This iron(II) oxidation causes domestic issues such as reddish color, staining of laundry, and solids deposition in the water leading to high turbidity. Aerial oxidation of iron(II) can further contribute to the growth of bacterial micro-organisms in water, and bacterial thriving on elevated levels of this metal could be responsible for bad odor and an increase of unpleasant taste [2, 3]. In addition, bacterial proliferation is known to be responsible for serious domestic problems due to iron-compounds precipitation, leading with time to cloggings of pipes and softeners [4, 5], and even producing punctures and leakages in the water distribution system [2, 3, 6]. Moreover, although iron is a vital metal in hemoglobin, myoglobin as well as in some enzymes, the use of iron-rich ground waters for drinking without treatment can pose some risks to human health. Indeed, several health issues due to the high iron content in water were reported in the literature. Briefly, it was stated that elevated levels of iron may injure the hematopoiesis of bone marrow by damaging hematopoietic stem/progenitor cells, resulting in hemochromatosis; toxic substances can then be liberated in human body, deteriorating vital organs, and consequently, being able to cause with time grave symptoms such as eye disorders, or even heart and cancer diseases [7-12]. Therefore, providing the population with safe drinking water becomes an important need and challenges worldwide. This explains why the Fe^{2+} removal process has gained emerging importance for obtaining standard drinking water in many countries. However, in some developing countries appropriate technologies for safe drinking water supply are, at best, present in urban areas, but not suitable in rural areas because all modern technologies possess disadvantages such as high cost, difficult maintenance, and high energy requirements.

Several techniques were employed in the past for removing soluble iron from waters, ***e.g.*** : (i) oxidation by using the oxygen in air as an oxidizing agent, accompanied by a separation / filtration mainly with sand ([2, 3, 13]; (ii) oxidation with various chemical oxidizing agents such as potassium permanganate, chlorine, and/or chlorine dioxide followed by (micro)-

filtration [13-20]; (iii) biological and/or physicochemical iron oxidation [21-24]; (iv) ion exchange with synthetic resins [2, 25]; (v) ultra-filtration/micro-filtration membranes [26-33]; bioremediation by employing micro-organism metabolism [35-38]; (vi) supercritical fluid extraction [39]; (vii) electric discharge treatment [40-42]; and viii) ozonation [43-47]. Even though adsorption is not a new purification method, recent technologies using low-cost adsorbents have made adsorption an increasingly economical and good purification process. Adsorption method was thus employed in the removal of iron from aqueous solutions by means of different natural or synthetic materials such as ash [48]; activated carbon ([49, 50] and references therein); dolomite [51]; kaolinite and /or montmorillonite [52-54]; natural zeolites and/or modified zeolites [55-63].

Zeolites were commonly used for drinking water and groundwater treatments, and particularly as softeners [64, 65]. Their use results from their high surface areas and good cation-exchangeable and molecular sieve properties. Zeolitic materials are hydrated alumino-silicate minerals consisting of three-dimensional frameworks of SiO_4 and AlO_4 tetrahedra. Their general chemical formula is given by:

$$M_{m/n}\,[(AlO_2)_x.(SiO_2)_y].zH_2O \qquad (1)$$

where M represents an exchangeable cation (a monovalent ion such as Na^+, K^+, and Li^+ or divalent ions such as Ca^{2+}, Mg^{2+}, Ba^{2+}, and Sr^{2+}); n corresponds to the cation charge and m the number of M cations in the zeolitic structure; and z is the number of water molecules [66, 67]. It is important to note that, depending upon the type of zeolite considered, the atomic ratio y/x in formula (1) varies from 1 to 6.

The main objective of this work was to examine the possibility of using zeolitized brick for improving the quality of ground waters in rural zones of the Central African Republic. For that purpose, the zeolitization of the brick was carried out under different alkaline (NaOH) conditions and by heating the reaction medium. Alkaline brick samples were analyzed by ESM/EDS in order to observe new crystalline specimens formed at brick surfaces, to study their morphology, and to evaluate their elemental composition. Batch experiments were performed at different temperatures, and results at equilibrium were interpreted by using the equilibrium adsorption isotherms proposed by Langmuir, Freundlich, and Dubinin-Radushkevich. ^{1}H and ^{23}Na MAS NMR were used for evidencing the role of water protons and sodium ions in Fe(II) adsorption. To gain information about the binding process,

thermodynamic parameters of iron(II) adsorption were calculated from the equilibrium constants derived from the distribution coefficient and partition coefficient. A consideration of the correct calculation of the thermodynamic parameters of iron(II) adsorption on to alkaline brick was made.

2. MATERIALS AND METHODS:

2.1. Adsorbents preparation

The raw brick used in this study came from Bangui region in the Central African Republic. The mineralogy of this brick was determined by means of X-ray diffraction (XRD) and chemical analyses [68]: 60-65 wt % quartz (SiO_2) and 20-25 wt % metakaolinite ($2SiO_2.Al_2O_3$); and to a lesser extent: 4-5 wt % illite; ≤ 4 wt % iron oxides / hydroxides; and ≤ 3 wt % feldspar + mica + biotite. Before use as an adsorbent, several physical/chemical treatments were carried out on the brick. First, it was broken into grains and sieved with sizes ranging from 0.7 to 1.0 mm. Second, brick pellets were treated in our laboratory under the following alkali conditions: 10 g of Bangui brick reacted in 40 mL of a diluted NaOH solution (0.2; 0.4; 0.6; and 0.8 $mol.L^{-1}$) at room temperature for one night under slow shaking at a speed of 120 rpm. This procedure was afterward followed by a fixed-temperature increase of the mixture at 90°C for a constant reaction time of six days. The recovered grains were afterward rinsed several times with MilliQ water and dried at 90°C for 24 hours. In this article, zeolitized Brick (ZB) samples were named: ZB1, ZB2, ZB3, ZB4, and ZB5 when treating the brick with the following NaOH concentrations: 0.2, 0.4, 0.6, 0.8 and 1.0 $mol.L^{-1}$, respectively.

2.2. Chemicals

All chemicals employed in the experiments were analytical grades. Sodium hydroxide and $FeCl_2.4H_2O$ were supplied by DIS LAB (France).

2.3 Isotherm study

To study the adsorption behavior of iron (II) ions on alkaline brick, the experiments for adsorption isotherms were performed at room temperature and under constant stirring condition. Isotherm study was carried out on brick grains with 0.7 -1.0 mm sizes. These experiments were performed in ten 100mL-flasks –each one containing 0.5 g of brick

pellets— in which were added 50 mL of an iron(II) solution with a concentration ranging from $5.71x10^{-4}$ to $1.46x10^{-3}$ mol.L^{-1}. These flasks were placed on a mechanical (orbital) shaker (Model: IKA Labortechnik KS 250 basic) and gently shaked at a speed of 120 rpm. Adsorption-isotherm experiments lasted one night although a reaction time of 4 hours at a temperature of 17°C ± 1°C was sufficient for the system to attain thermodynamic equilibrium. Afterward, suspensions were filtered and recovered solutions were analyzed in order to determine iron concentrations using an ICP-AES (Inductively Coupled Plasma Atomic Emission Spectroscopy; Model: Varian Pro axial view) spectrometer. The metal uptake and percentage removal were calculated using the relationships:

$$Q_e = \frac{(C_o - C_e).V}{m} \quad (2)$$

$$\%adsorption = \frac{(C_o - C_e)}{C_o} x100\% \quad (3)$$

where C_o (mg.L^{-1}) and C_e (mg.L^{-1}) are the initial and equilibrium concentrations of iron(II), respectively; V (L) is the volume of the aqueous solution used in batch experiments, and m (g) is the mass of alkaline brick added in the solution. It should be noted that all these experiments were at least triplicated and data were averaged.

2.3. X-ray diffraction study

XRD patterns were conducted at room temperature in a Bruker D8 Advance diffractometer using Ni-filtered CuKα radiation (40kV, 40 mA). Samples were scanned with a step size of 0.02° and a counting time of 0.5 sec per step.

2.3. Solid - state NMR study

The ^{1}H and ^{23}Na MAS-NMR spectra were recorded at 800 and 211.7 MHz, respectively, on an 18.8 T Bruker Avance III spectrometer equipped with a Bruker 3.2 mm CP-MAS probe operating at a ν_{rot} of 20 kHz. The ^{23}Na (I = 3/2) MAS-NMR experiments were recorded with a pulse length of 1 µs (~ π/5 flip angle), 1024 transients, and a recycle delay of 2 s. The ^{1}H MAS-NMR experiments were recorded with a π/2 pulse length of 3.5 µs, 128 transients and

a 5s rd using the DEPTH sequence in order to suppress the signal coming from the measurement probe.

The ^{1}H and ^{23}Na chemical shifts were referenced as 0 ppm to TMS and NaCl solution (1 mol.L^{-1}), respectively.

3. RESULTS AND DISCUSSION:

3. 1. Alkaline bricks characterization

The x-ray diffraction pattern of raw brick inferred the existence of mainly quartz and, to a lesser extent, illite and rutile (not shown here). After treating Bangui brick with sodium hydroxide at 90°C for 6 days, it was found that, during the course of the heterogeneous reaction, the NaOH concentration was found to be a relevant parameter in the crystalline transformation of the brick. Indeed, as shown in Fig. 1 the diffractograms of the brick treated with 0.2 mol.L^{-1} NaOH (noted ZB1) display new XRD peaks with very low intensities, in addition to those ascribed to crystalline brick minerals.

The intensity of these new peaks increased in the diffractogram of the brick treated with 0.4 mol.L^{-1} NaOH (noted ZB2; Fig. 1).

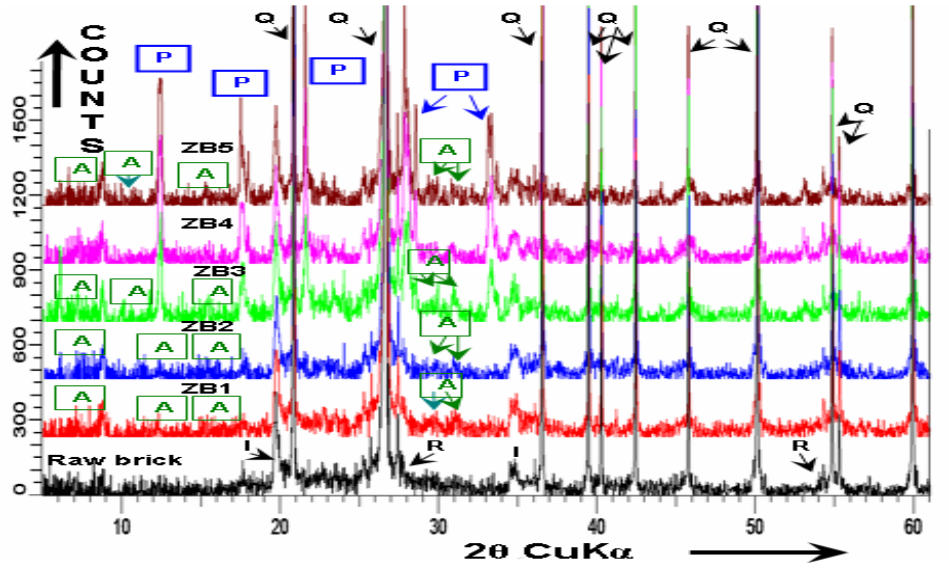

Figure 1: X-ray diffractograms of raw brick and 'zeolitized' bricks (ZB). ZB samples were synthesized under different alkaline conditions at 90°C for 6 days by using the following NaOH concentrations: 0.2 mol.L^{-1}, ZB1; 0.4 mol.L^{-1}, ZB2; 0.6 mol.L^{-1}, ZB3; 0.8 mol.L^{-1}, ZB4; and 1.0 mol.L^{-1}, ZB5. A NaA zeolite; P, NaP zeolite; Q, quartz; R, rutile; I, illite.

As for the diffractogram of the brick treated with 0.6 mol.L^{-1} NaOH (noted ZB3; Fig. 1), these new XRD peaks appeared much better and were further accompanied with other reflections. The XRD patterns of the recovered brick samples (ZB1, ZB2, and ZB3) indeed displayed at least five main characteristic peaks at 2θ: 7.2°, 12.5°, 16.1°, 30.0° and 30.8° corresponding to Miller indices (200), (200), (420), (644 and 820) and (822 and 660), respectively (see Fig. 1) [69];. This observation confirmed the presence of the LTA zeolite as the major new crystalline phase generated in the brick. As for the recovered ZB4 and ZB5 samples, their X-ray diffraction patterns inferred the predominance of NaP zeolite due to the detection of the following (main) diffraction peaks (2θ): 12.5°, 17.7°, 21.7°, 28.1°, and 33.4° corresponding to Miller indices (101), (200 and 002), (211, 112 and 121), (310, 301, and 103) and (213, 312, and 321), respectively ([69] (see Fig. 1). It is worth noting that the latter diffraction peaks were also detected in the ZB3 sample but with lowest intensity heights, suggesting that ZB3 contains mostly NaA crystals and, to a lesser extent, some NaP crystals, as evidenced by ESEM analysis (see below).

The surface structure/morphology and dispersion of zeolitic particles were explored by using the ESEM/EDS technique. The ESEM image of raw brick showed that this material contains mainly quartz crystals associated with aluminosilicate aggregates (clays) with surface roughness and cracks (not shown here).

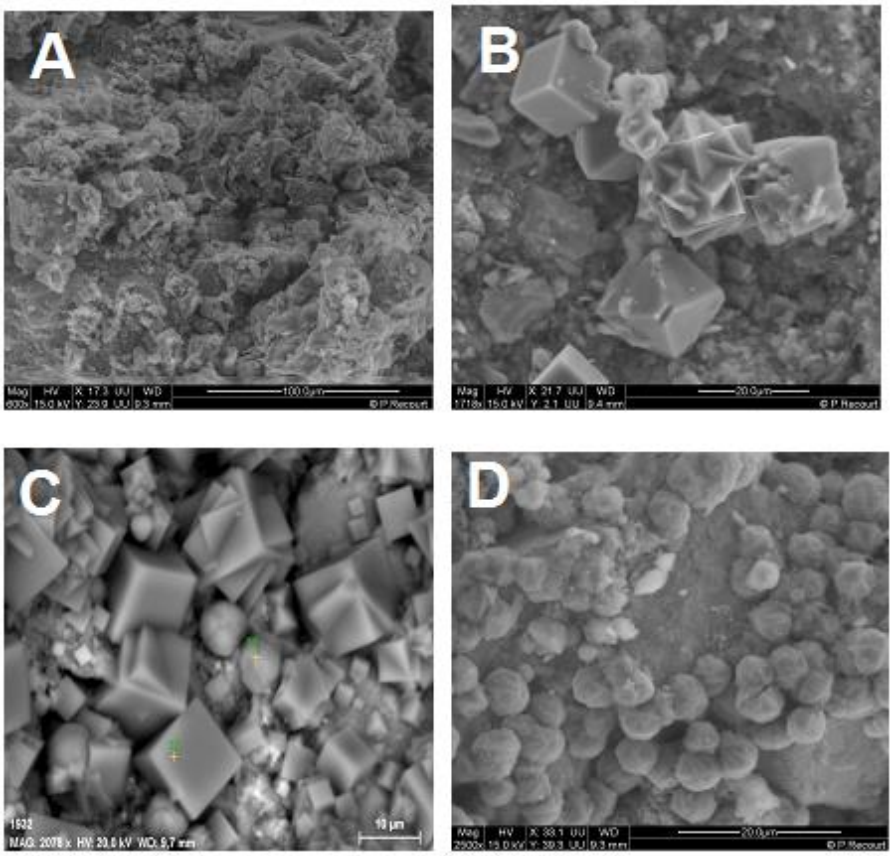

Figure 2: ESEM micrographs of 'zeolitized' bricks (ZB). ZB samples were synthesized under alkaline conditions at 90°C for 6 days by using the following NaOH concentrations: (A) 0.2 mol.L^{-1}, ZB1; (B) 0.4 mol.L^{-1}, ZB2; (C) 0.6 mol.L^{-1}, ZB3; and (D) 0.8 mol.L^{-1}, ZB4.

In Fig. 2, when compared to ESEM image of untreated brick, ESEM image An obtained for the ZB1 sample (brick treated with 0.2 mol.L^{-1} NaOH) displayed an intense deposition of aluminosilicate gels considered as a precursor non-crystalline phase and possessing the same (or close) chemical composition as those of zeolites NaA and NaP (which were detected under higher alkaline conditions as shown in ESEM images B, C and D of Fig. 2).

ESEM image B obtained for the ZB2 sample (brick treated with 0.4 mol.L^{-1} NaOH) revealed the presence of new micro-specimens at the surfaces of alkaline-brick grains with cubic shapes and sizes ranging from 5 to 10 µm. These cubic crystals were found to be comparable with those observed previously for the A-type zeolite by the SEM technique [63, 70]. ESEM image C obtained for the ZB3 sample (brick treated with a 0.6 mol.L^{-1} NaOH solution) showed the occurrence of some spherical shape crystals with diameter sizes varying from 3 to 6 µm in addition to cubic crystals. These spherical shape crystals were identified as zeolite

NaP, and they were further found to be comparable with those reported in the literature [71-74]. As for the ZB4 sample (brick treated with 0.8 mol.L^{-1} NaOH), its ESEM micrograph (see ESEM image D of Fig. 2) exhibited only spherical shape crystals, indicating the total transformation of NaA zeolite into NaP zeolite under our specific alkaline conditions. A similar ESEM image as that of ZB4 was observed for the ZB5 sample (not shown here).

In what follows, only ZB1, ZB2, ZB3, and ZB4 were tested as adsorbents for Fe(II) adsorption from aqueous solutions.

3.2. Adsorption isotherms

In batch experiments and in order to interpret the adsorption characteristics of adsorbents, Langmuir, Freundlich, and Dubinin-Radushkevich (D-R) isotherm models are the commonly used models by scientists. Adsorption-isotherm equations express the relationship between the equilibrium adsorption quantity of the adsorbent and the equilibrium concentration of the adsorbate at a constant temperature.

Batch mode experiments on adsorption of iron (II) by zeolitized brick samples noted ZB1, ZB2, ZB3, and ZB4 (as pointed out in the Experimental Section), were conducted at room temperature. In this work, Fe(II) Adsorption by alkaline brick was modeled by using Langmuir and Freundlich and Dubinin-Radushkevich (D-R) isotherms.

3.2.1 Langmuir isotherm

To apply this model to our system, we assumed that: *first* Fe(II) adsorption would take place at specific homogeneous active sites of the brick; *second* these sites ought to be energetically identical at the brick surface.

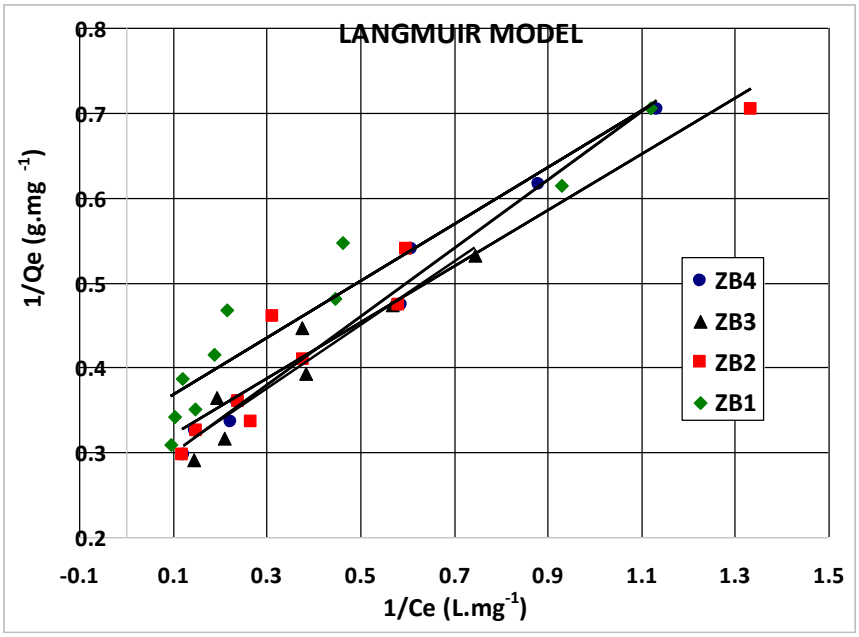

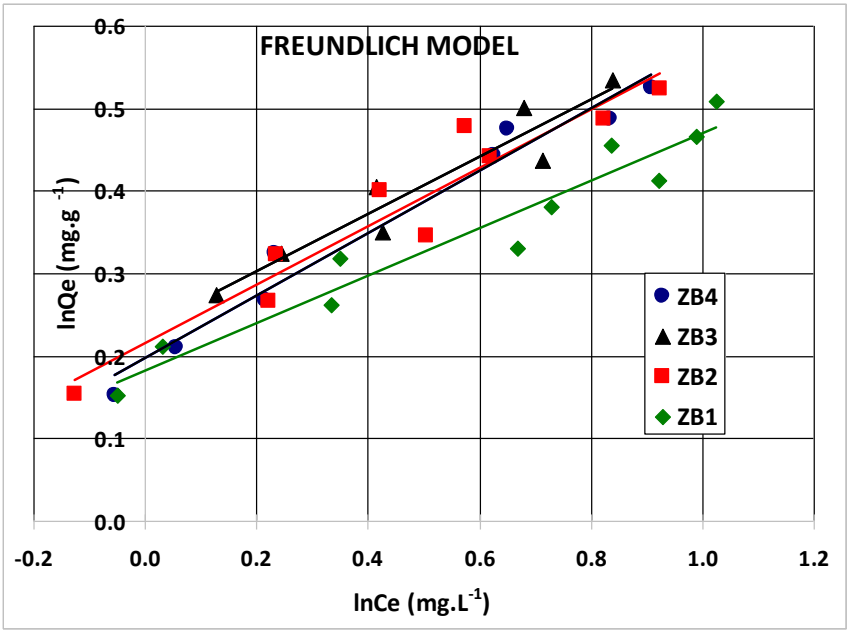

Figure 3: Langmuir and Freundlich's isotherms obtained for iron(II) adsorption by 'zeolitized' bricks (ZB). ZB samples were synthesized under alkaline conditions at 90°C for 6 days by using the following NaOH concentrations: 0.2 mol.L^{-1}, ZB1; 0.4 mol.L^{-1}, ZB2; 0.6 mol.L^{-1}, ZB3; and 0.8 mol.L^{-1}, ZB4.

The linearized mathematical form of the Langmuir equation is given by [75, 76]:

$$\frac{1}{Q_e} = \frac{1}{K_L.Q_{max}.C_e} + \frac{1}{Q_{max}} \qquad (4)$$

where K_L (L.mg^{-1}) is the Langmuir constant that depends upon the energy of adsorption of the alkaline brick towards iron(II); Q_{max} (mg.g^{-1}) the maximum adsorption capacity; Q_e (mg.g^{-1}) the amount of Fe^{2+} ions adsorbed on to zeolitized brick grains leading to the formation of monolayer on the brick surface; and C_e (mg.L^{-1}) the equilibrium concentration of Fe^{2+} ions in the liquid phase. The plots of $1/Q_e$ against $1/C_e$ give straight lines (Fig. 3). The Langmuir constant and the maximum adsorption capacity were calculated from the slopes and intercepts of the plottings. We found K_L values varying from 0.641 to 0.997 L.mg^{-1} and Q_{max} values from ~3.0 to ~3.9 mg.g^{-1}, see Table 1. The Q_{max} values indicate better binding of Fe^{2+} ions on alkaline bricks in the following order: ZB1 < ZB2 < ZB3 < ZB4 (Fig. 4).

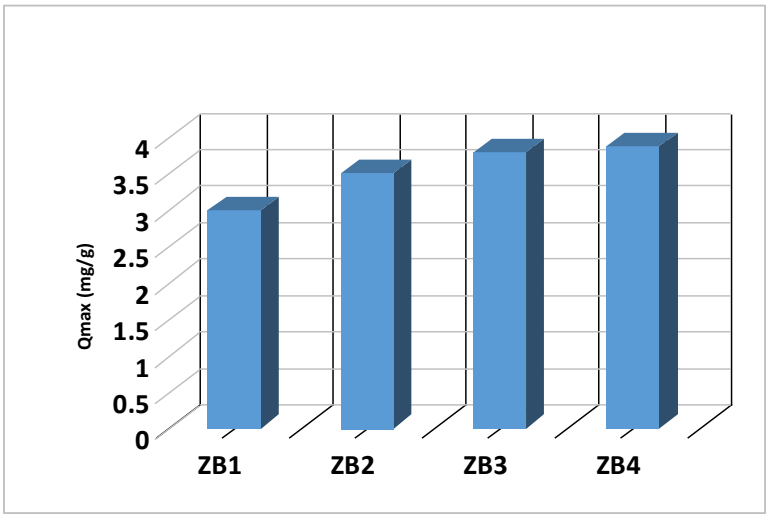

Figure 4: Evolution of the maximum Fe(II)-adsorption capacity, Q_{max} (mg.g^{-1}), of the brick which was previously treated with increasing NaOH concentrations ranging from 0.2 to 0.8 mol.L^{-1}.

This finding might be explained by the abundance of zeolitic particles coating brick pellets that increased when the NaOH concentration in the reaction medium increased from 0.2 mol.L^{-1} to 0.8 mol.L^{-1} (as evidenced by ESEM/EDS analysis; see section 3.1). This observation might explain the maximum adsorption capacity, Q_{max}, attained by employing the ZB4 brick as an adsorbent for iron(II) adsorption, as shown in Fig. 4. The regression coefficients (R^2) ranged from 0.904 to 0.987 (see table 1), revealing a good fitting of theoretical data when applying the Langmuir model to experimental ones.

Table 1: Langmuir and Freundlich isotherms parameters obtained for iron(II) adsorption by zeolitized bricks (ZB).

	Langmuir model				Freundlich model		
Alkaline bricks	**Qmax ($mg.g^{-1}$)**	**K_L ($L.mg^{-1}$)**	**R_L**	**R^2**	**K_F $mg.g^{-1}$**	**n_F**	**R^2**
ZB1	2.99745	0.997	0.01-0.03	0.9090	0.8338	3.476	0.9389
ZB2	3.4928	0.872	0.01-0.03	0.9206	0.8063	2.829	0.9167
ZB3	3.7905	0.697	0.02-0.04	0.9045	0.7917	2.891	0.9127
ZB4	3.8698	0.641	0.02-0.05	0.9866	0.8217	2.639	0.9692

In order to reveal the feasibility of Fe(II) adsorption on to zeolitized brick, the dimensionless separation factor, R_L [77, 78], was applied to our system. This parameter is indeed considered as an indicator of the adsorption nature by classifying the isotherm to be: (i) either favourable if $0 < R_L < 1$; linear if $R_L = 1$; unfavourable when $R_L > 1$; or irreversible when $R_L = 0$. It can be determined from the equation:

$$R_L = \frac{1}{1 + K_L.C_o} \qquad (5)$$

where C_o ($mg.L^{-1}$) is the initial adsorbate quantity; and K_L ($L.mg^{-1}$) the Langmuir sorption constant described above. In this study, the R_L values ranged from 0.01 to 0.05 (see table 1), indicating the favourability of Fe(II)-adsorption process at room temperature.

3.2.2 Freundlich model

In this model, it was assumed that Fe(II) adsorption would occur as multilayer adsorption on heterogeneous surfaces of alkaline brick. The linearized form of the Freundlich equation is given by [79]:

$$\ln Q_e = \ln K_F + (\frac{1}{n_F}).\ln C_e \qquad (6)$$

where K_F ($mg.g^{-1}$) and n_F are Freundlich isotherm constants corresponding to multilayer adsorption capacity and adsorption intensity, respectively. The plots of $\ln Q_e$ against $\ln C_e$ yield straight lines (Fig. 3). Freundlich equilibrium constants could be calculated from the slopes and intercepts of the plottings. We found K_F values varying from 0.7917 to 0.8338 $mg.g^{-1}$ and n_F values varying from 2.639 to 3.476, see Table 1. The regression coefficients

(R^2 = 0.9127-0.9692) were slightly lower than those obtained from the Langmuir equation, indicating barely the lowest fitting of adsorption data for iron(II) to Freundlich model. The slope $1/n_F$ is used as a heterogeneity factor. Indeed, the adsorption becomes heterogeneous as far as the $1/n_F$ value becomes close to 0; whereas if the slope $1/n_F$ is > 1, adsorption is a physical process; and if $1/n_F$ < 1, adsorption is considered more as a chemical process [80]. In this study, all the $1/n_F$ values were found to be between 0.288 and 0.379, suggesting that the removal of iron(II) by alkaline brick occurred mostly according to a chemical adsorption process.

From the above results, it could be concluded that the adsorption of Fe^{2+} ions on to zeolitized brick occurred more according to the Langmuir isotherm model at specific homogeneous active sites of the brick. Indeed, when compared to Freundlich model data, monolayer adsorption capacities calculated by using the Langmuir model (Q_{max}) were found to be much closer to those determined directly from experimental results (Q_{exp}).

3.2.3 Dubinin-Radushkevich (D-R) isotherm

To assess the nature of bonding between Fe^{2+} ions and the alkaline-brick adsorbent, the D-R isotherm was applied to our system. The linear form of the D-R isotherm is given by [81]:

$$\ln Q_e = \ln Q_{D-R} - \beta.\varepsilon^2 \qquad (7)$$

where Q_{D-R} ($mg.g^{-1}$) represents the theoretical saturation capacity of alkaline brick; β ($mol^2.kJ^{-2}$) is a constant relative to the mean free energy of adsorption per mole of iron(II), and ε corresponds to the Polanyi potential. In order to evaluate the adsorption potential, ε, a more systematic approach had previously been presented for ion exchange/adsorption of metals and adsorption of dyes from aqueous solutions using several adsorbents [82-86]. From Inglezakis' works [87], solubility-normalized Dubinin–Astakhov adsorption isotherm for ion-exchange systems was applied in this study, and the Polanyi (adsorption) potential, ε, was calculated from the equation:

$$\varepsilon = RT \ln(1 + \frac{1}{C_e}) \qquad (8).$$

where C_e ($g.g^{-1}$) is the equilibrium concentration of the solute in the solution. The plots of $\ln Q_e$ against ε^2 yield straight lines (Fig. 5), and their slopes and intercepts permit the

calculation of β and Q_{D-R}, respectively. We found: β = -2.00.10^{-9} mol^2.kJ^{-2} and Q_{D-R} = 21.28 mg.g^{-1} for ZB4; β = -2.00.10^{-9} mol^2.kJ^{-2} and Q_{D-R} = 19.25 mg.g^{-1} for ZB3; β = -1.00.10^{-9} mol^2.kJ^{-2} and Q_{D-R} = 3.874 mg.g^{-1} for ZB2; and β = -1.00.10^{-9} mol^2.kJ^{-2} and Q_{D-R} = 3.555 mg.g^{-1} for ZB1.

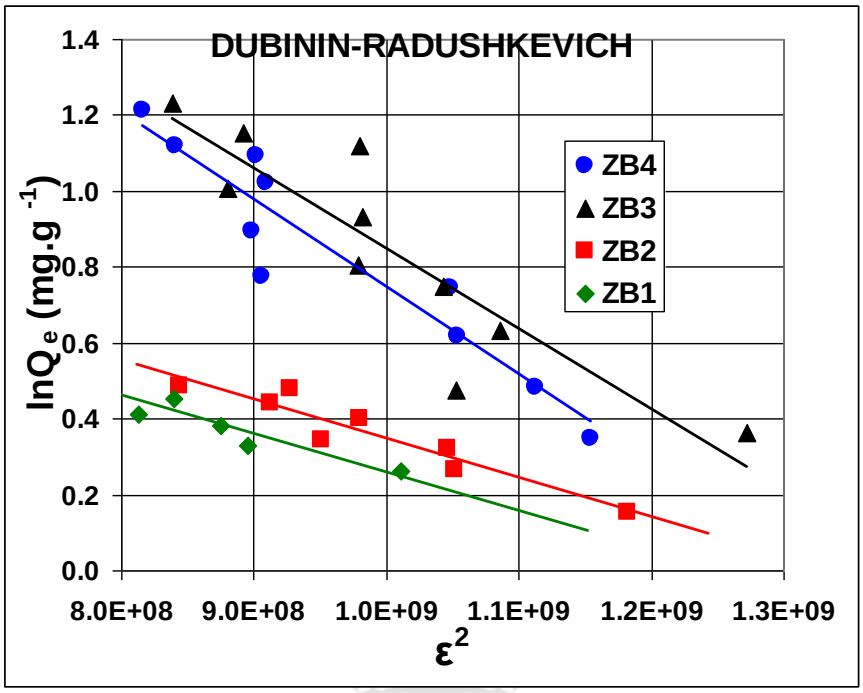

Figure 5: Dubinin-Radushkevich isotherms obtained for iron(II) adsorption by 'zeolitized' bricks (ZB). ZB samples were synthesized under alkaline conditions at 90°C for 6 days by using the following NaOH concentrations: 0.2 mol.L^{-1}, ZB1; 0.4 mol.L^{-1}, ZB2; 0.6 mol.L^{-1}, ZB3; and 0.8 mol.L^{-1}, ZB4.

The Q_{D-R} value for Fe^{2+} adsorbed on to ZB4 was much higher than those obtained with ZB1 and ZB2 as adsorbents, and slightly higher than that for Fe^{2+} adsorbed on to ZB3, confirming the better adsorptive properties of NaP coatings at ZB4 surfaces. The changes in free energy, E_{D-R}, involved for the transfer of one mole of Fe^{2+} ions from infinity towards the surface of alkaline-brick pellets were determined from the β values by using the mathematical expression (see ref. [87] and references therein):

$$E_{D-R} = \frac{1}{\sqrt{-2\beta}} \qquad (9).$$

We found E_{D-R} = 22.4 kJ.mol^{-1} for both ZB1 and ZB2 and E_{D-R} = 15.8 kJ.mol^{-1} for both ZB3 and ZB4. For alkaline brick grains being well coated with NaA and/or NaP zeolites (*i.e.*, the

ZB3 and ZB4 samples; see ESEM images C and D of Fig. 2), the E_{D-R} value obtained (E_{D-R} = 15.8 kJ.mol^{-1}) is in the order of those expected for an ion-exchange mechanism in which the sorption energy lies within 8-16 kJ.mol^{-1} [86, 88-91]. Again, this result confirmed that the adsorption of Fe^{2+} ions on zeolitized-brick surfaces refers to a chemisorption mechanism which is similar to that predicted from the Freundlich isotherm model (see above).

It is, however, worth noting that the regression coefficients relative to the linear plots $\ln Q_{D-R}$ vs ε^2 were somewhat weak (R^2 ranging from 0.799 to 0.9054), and thereby, Fe(II)-adsorption data seemed to fit less to D-R isotherm model than to Langmuir and Freundlich isotherm models.

In the other hand, from batch-experiments data obtained for Fe(II) adsorption on zeolitized bricks (ZB1, ZB2, ZB3, and ZB4), the equilibrium concentration of brick sodium released in the liquid phase was plotted against the equilibrium concentration of Fe^{2+} ions deposited on to brick surfaces (Fig. 6).

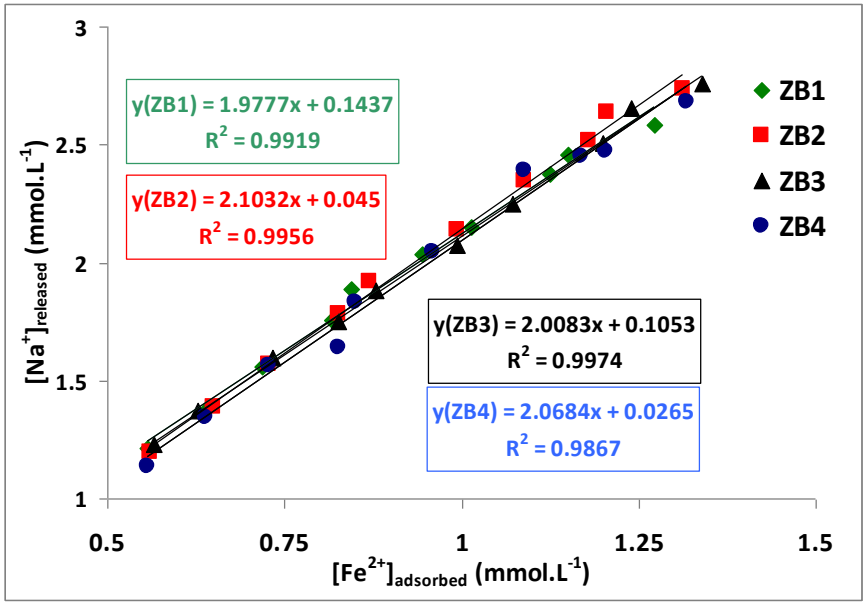

Figure 6: The equilibrium concentration of brick sodium released in the liquid phase as a function of the equilibrium concentration of Fe^{2+} ions deposited on to different 'zeolitized' bricks (ZB). ZB samples were synthesized under alkaline conditions at 90°C for 6 days by using the following NaOH concentrations: 0.2 mol.L^{-1}, ZB1; 0.4 mol.L^{-1}, ZB2; 0.6 mol.L^{-1}, ZB3; and 0.8 mol.L^{-1}, ZB4.

All the fitting plots were found to pass nearly through the origin (the intercepts are close to zero: y = 2.0230(± 0.0454) + 0.0801(±0.0586)) and with good regression coefficients (R^2 ranging from 0.9867 to 0.9974; see Fig. 6). This finding supported the view that this process occurred stoichiometrically as an ion-exchange between two Na^+ ions coming from the brick surface and one Fe^{2+} ion present in the water column. Thereby, the quantity of Na^+ ions bound to the brick might be considered as a relevant indicator of the number of reactive (negatively charged) sites at the adsorbent surface. For calculations of equilibrium constants and thermodynamic parameters relative to our heterogeneous system (see section 3.3), we then assimilated the amount of sodium in synthesized brick to that of surface-brick sites, i.e.: $>S–O^-$ with S = Al or Si.

3.3 Feasibility and nature of the adsorption process

In this paragraph, the determination of equilibrium constants and thermodynamic parameters were assessed only for iron(II) adsorption on ZB3 and ZB4 because, in these two materials, the transformation of brick metakaolinite into zeolite(s) NaA and/or NaP was assumed to be complete.

3.3.1 Distribution coefficient (K_d)

The influence of temperature in the removal of iron(II) by zeolitized brick was examined in a view of the practical application in the field for the decontamination of Fe(II)-polluted ground waters at pilot scale in the Central African Republic. For that purpose, Fe(II) adsorption was performed at different temperatures including 293.15, 298.15, 303.15, and 308.15°K. In order to study adsorption thermodynamics of carbofuran on Sn(IV) arsenosilicate in H^+, Na^+ and Ca^{2+} forms, Khan and Singh [92] proposed in 1986 the use of a thermodynamic distribution coefficient, K_d (L/g), defined as:

$$K_d = \frac{Q_e}{C_e} \qquad (10)$$

where Qe and Ce are the equilibrium contents of iron(II) on the zeolitized brick and in the solution, respectively. This method had been used in the literature for the calculation of thermodynamic parameters [93-95]. Unfortunately, the unit of K_d is liter per gram. This unit problem had been discussed previously [96-98]. For instance, Milonjic [97] reported that numerous incorrect calculations of thermodynamic parameters, ΔS and ΔG, were published

in the literature, leading to erroneous interpretations/conclusions in contradiction to experimental data. To address this problem, several authors [97-100] proposed the use of a dimensionless constant, K_c, by multiplying K_d by a factor of 1000 corresponding to the solution density (assuming that the density of the aqueous phase used in batch experiments remains close enough to that of pure water *i.e.*, 1000 $g.L^{-1}$). The term $K_c(g.g^{-1}) = K_d(L.g^{-1})x1000(g.L^{-1})$ then becomes dimensionless.

Gibbs free energy change (ΔG°) was then calculated from the equation:

$$\Delta G^o = -RT \ln(K_c) \qquad (11).$$

The values of ΔG° were found to be negative for all studied temperatures (see Table 2). Increase in temperature and decrease in the value of free energy change (ΔG°) indicated that the iron(II) adsorption process was more favorable at higher temperatures. This suggested that the adsorption of iron(II) on to alkaline brick was thermodynamically spontaneous. The ΔG° values decreased from -15.758 $kJ.mol^{-1}$ to -22.636 $kJ.mol^{-1}$ for ZB3 and from -15.756 $kJ.mol^{-1}$ to -24.121 $kJ.mol^{-1}$ for ZB4 when the temperature was increased from 293.15°K to 308.15°K, revealing two features: *first* the degree of spontaneity increases with the increase in temperature, and *second* the system requires more amount of energy in order to facilitate the heterogeneous reaction.

From Van't Hoff equation, the thermodynamic distribution coefficient, K_c, can be expressed as a function of temperature according to:

$$\ln K_c = \frac{\Delta S^o}{R} - (\frac{\Delta H^o}{R}).(\frac{1}{T}) \qquad (12)$$

where ΔH° and ΔS° are the enthalpy change and entropy change, respectively. By plotting $Ln(K_c)$ against 1/T, we obtained straight lines (see Fig. 7). The values of ΔH° and ΔS° were then determined from the slopes and the intercepts of the plots of $Ln(K_c)$ vs 1/T. We found: ΔH° = +111.738 $kJ.mol^{-1}$ and ΔS° = +436.152 $J.mol^{-1}.K^{-1}$ for ZB3 and ΔH° = +147.947 $kJ.mol^{-1}$ and ΔS° = +559.045 $J.mol^{-1}.K^{-1}$ for ZB3 (see Table 2). The positive values of ΔH° indicated that the process is endothermic, which is confirmed by the increasing adsorption of Fe^{2+} ions by alkaline brick with an increase in temperature.

Generally, a low enthalpy change value of $\Delta H° < 20$ kJmol^{-1} indicates that physisorption is involved in the studied system, while in the case of chemisorption the $\Delta H°$ value ranges from 80 and 400 kJ.mol^{-1}, as pointed out previously [95, 101, 102]. The estimated values of $\Delta H°$ for the present system were found to be higher than 80 kJmol^{-1} (with $\Delta H°$ varying from +111.738 to +147.947 kJ.mol^{-1}), indicating the involvement of an ion-exchange (chemisorption) succeeding to electrostatic attraction (physisorption) between Fe^{2+} ions (in the liquid phase) and negatively charged surface (on the brick) during the iron(II)-adsorption mechanism. The highly positive values of the entropy change (with $\Delta S°$ varying from +436.152 to +559.045 J.mol^{-1}.K^{-1}) were consistent with an increase in randomness and in the degrees of freedom of the implicated species at the brick-water interface as a result of chemical surface modifications.

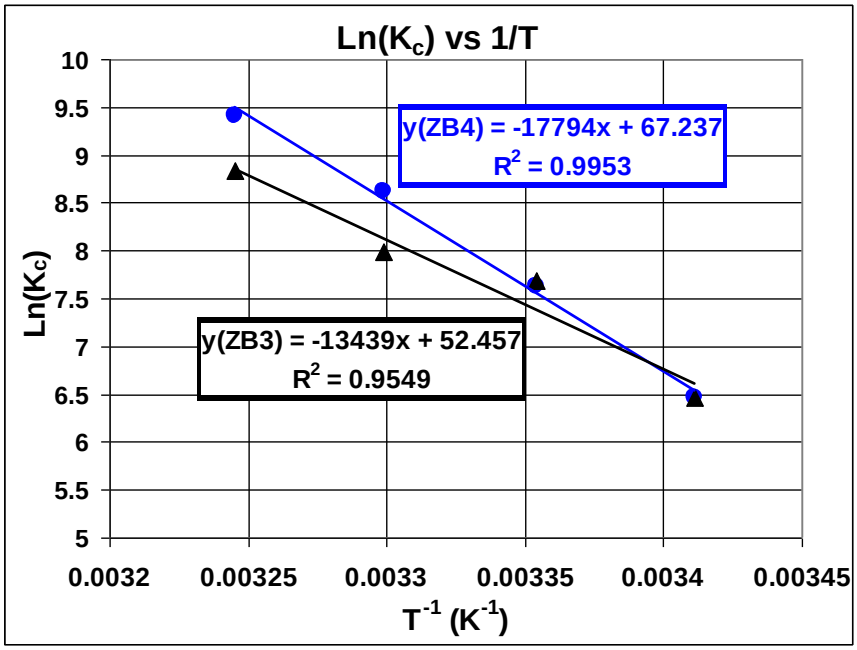

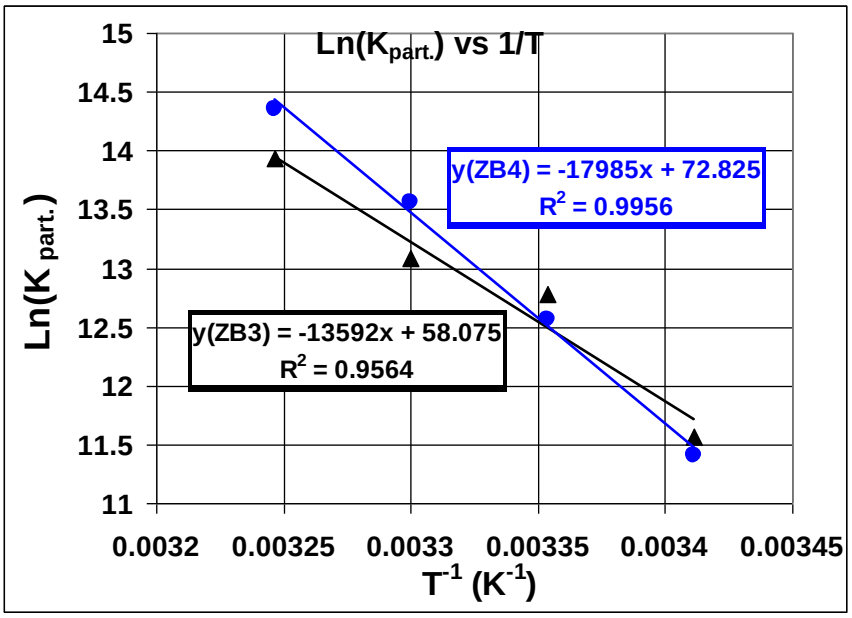

Figure 7: Thermodynamic distribution and partition coefficients, K_c and $K_{part.}$, expressed as a function of temperature (according to Van't Hoff equation).

Indeed, chemical surface reactions were assumed to occur: *first* when water molecules were released from $Fe(H_2O)_6^{2+}$ ions and/or hydrated zeolitic pores during the migration of Fe^{2+} ions from the liquid to the brick surface owing to the existence of electrostatic forces at the brick-water interface; and *second* when $Na(H_2O)_n^+$ was removed from ion-pairs (>S–O^----$(H_2O)_n$---Na^+, where >S–O^- represents an active site of the brick zeolite) in order to balance electric charges at the brick-water interface.

3.3.2 Thermodynamic partition coefficient ($K_{part.}$)

As reported in the literature and according to the United States Environmental Protection Agency, the partition coefficient might be used as a thermodynamic equilibrium constant if the initial concentration of the adsorbate is weak. Because of the low concentrations of iron (II) used in batch experiments, the partition coefficient might be employed here for calculation of thermodynamic parameters relative to our heterogeneous water/alkaline-brick system.

The partition coefficient ($K_{part.}$) is defined as [102, 103]:

$$K_{part.} = \frac{a_{Fe}(brick)}{a_{Fe}(sol.)} \qquad (13)$$

where a_{Fe}(brick) represents the activity of the adsorbed iron(II) on to alkaline brick, and a_{Fe}(sol.) the activity of iron(II) in the solution at the equilibrium state. In our calculation, "activity" was assimilated to "molar fraction". Hence, the activity of iron (II) in the brick could be approximated as:

$$a_{Fe}(brick) = \frac{X_{Fe}(brick)}{X_{Na}^{Total}(brick)} \qquad (14)$$

where X_{Fe}(brick) and $X_{Na}^{Total}(brick)$ represent the molar contents of Fe^{2+} and Na^{+} per gram of brick zeolite [$X_{Na}^{Total}(brick)$ also represents potentially the total number of sodic sites per gram of material at brick surfaces before carrying out iron(II) adsorption]. After performing total acid attacks of alkaline bricks, ICP-AES analysis of recovered solutions allowed the assessment of the $X_{Na}^{Total}(brick)$ value. As for the activity of iron adsorbed in the brick, X_{Fe}(brick), it was determined from the relationship:

$$X_{Fe}(brick) = \frac{(C_o - C_{sol.}).V}{1000.m_{brick}.M_{Fe}} \qquad (15)$$

Where C_o represents the initial concentration of iron (II) in the solution ($mg.L^{-1}$) in contact with the brick during batch experiments, and $C_{sol.}$ is the concentration of iron (II) in the solution at equilibrium ($mg.L^{-1}$); V (in liter) corresponds to the volume of iron (II) solution used for batch experiments; m_{brick} the mass of brick employed (g); and M_{Fe} the atomic mass of iron ($g.mol^{-1}$).

The activity of iron (II) in the solution was estimated from the equation:

$$X_{Fe}(sol.) = \frac{C_{sol.}.V}{1000.M_{Fe}.55.55} \qquad (16)$$

where the factor 55.55 corresponds to the number of moles of pure water per liter or 1000 g at 298°K (*i.e.* by considering the ratio:$1000/M_{water}$ = 55.55 with M_{water} =18 $g.mol^{-1}$).

Gibbs free energy change (ΔG°) was then calculated from the equation:

$$\Delta G^{o} = -RT \ln(K_{part.}) \qquad (17).$$

The ΔG° values were reported in Table 2. These values show that the process is favorable at higher temperatures.

Table 2: Thermodynamic parameters relative to iron(II) adsorption by zeolitized bricks (ZB3 and ZB4), calculated from distribution coefficient (K_c) and partition coefficient ($K_{part.}$) at different reaction temperatures.

Alkali brick	Distribution coefficient (K_c)					
	ΔH° kJ.mol^{-1}	**ΔS° J.mol^{-1}K^{-1}**	**ΔG° at 293K kJ.mol^{-1}**	**ΔG° at 298K kJ.mol^{-1}**	**ΔG° at 303K kJ.mol^{-1}**	**ΔG° at 308K kJmol^{-1}**
ZB3	+111.738	+436.152	-15.758	-19.042	-20.131	-22.647
ZB4	+147.948	+559.040	-15.756	-18.912	-21.720	-24.121
	Partition coefficient ($K_{part.}$)					
	ΔH° kJ.mol^{-1}	**ΔS° J.mol^{-1}K^{-1}**	**ΔG° at 293K kJ.mol^{-1}**	**ΔG° at 298K kJ.mol^{-1}**	**ΔG° at 303K kJ.mol^{-1}**	**ΔG° at 308K kJmol^{-1}**
ZB3	+113.009	+482.859	-28.186	-31.681	-32.972	-35.693
ZB4	+149.536	+605.501	-27.797	-31.158	-34.160	-36.760

From Van't Hoff equation, the thermodynamic partition coefficient, $K_{part.}$, can also be expressed as a function of temperature according to reaction (12). By plotting Ln($K_{part.}$) against 1/T, we obtained straight lines (see Fig. 7). The values of ΔH° and ΔS° were then determined from the slopes and the intercepts of the plots of Ln($K_{part.}$) vs 1/T. The thermodynamic parameters calculated from the partition coefficient were reported in Table 2. We found: ΔH° = +113.009 kJ.mol^{-1} and ΔS° = +482.859 J.mol^{-1}K^{-1} for ZB3, and ΔH° = +149.535 kJ.mol^{-1} and ΔS° = +605.501 J.mol^{-1}K^{-1} for ZB4. These values are somewhat close enough to those calculated from the distribution coefficient. The thermodynamic parameters calculated also indicate that the process is endothermic with an increase in randomness at the brick-water interface. It is interesting to note that in this case $K_{part.}$, ΔG°, ΔH°, and ΔS° were not dependent on the units (mg.L^{-1} or mmol.L^{-1}) relative to the Fe^{2+} ions concentration.

3.4 Mechanistic aspects of iron (II) adsorption on to an alkaline brick

3.4.1Chemical iron (II) speciation

Identification of chemical forms of iron ionic species interacting with zeolite-crystals surfaces was greatly helpful in elucidating the mechanism involved at the brick-water interface. For that purpose, chemical Fe(II) speciation in water was undertaken under batch experiment conditions. Fe(II)-speciation data were obtained by the Visual MINTEQ program and presented graphically in Fig. 8. Globally, speciation results revealed that iron was present in its free ionic form up to pH~ 8.2, and beyond pH ~ 11 the dominant species was $Fe(OH)_3^-$. Intermediately at pH > 8, free Fe^{2+} ions started hydrolyzing as iron(II) was converted mainly into $Fe(OH)^+$ and $Fe(OH)_{2(aq.)}$. These intermediate Fe(II) species attained a maximum proportion of 71.68% at pH~10 for $Fe(OH)^+$, and 17.47% at pH ~11 for $Fe(OH)_{2(aq.)}$.

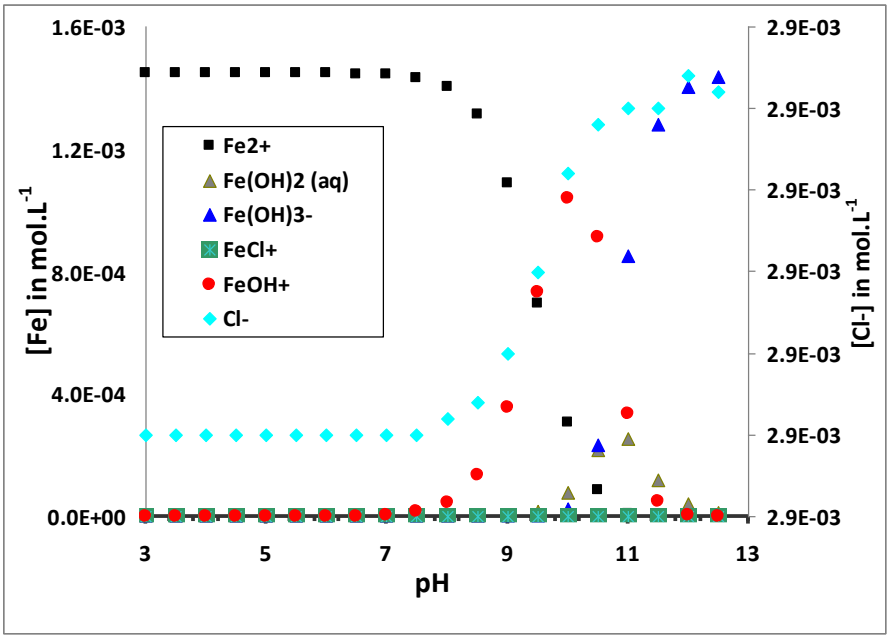

Figure 8: Distribution of the various iron(II) species in water under batch experiment conditions.

3.4.2 pH-dependence adsorption

The pH-dependence data on iron(II) adsorption by alkaline brick grains were presented graphically in Fig. 9.

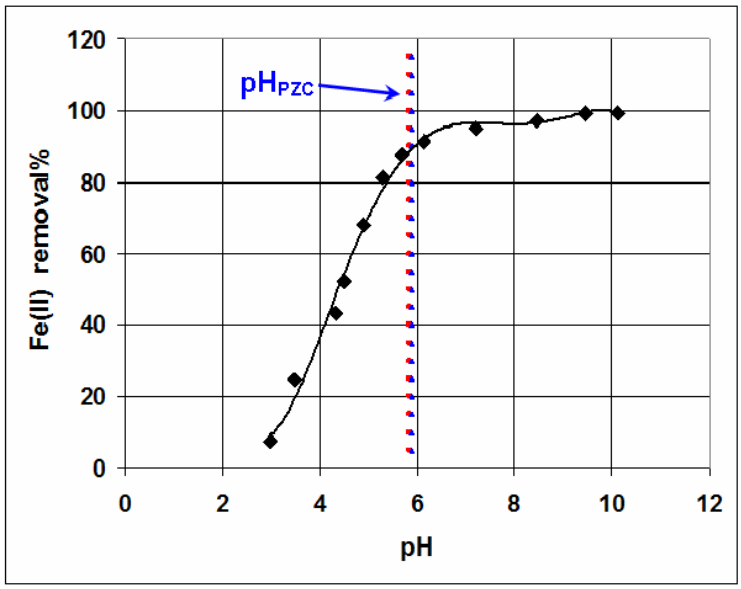

Figure 9: Influence of pH on the percent adsorption of Fe(II) from aqueous solutions by zeolitized brick.

During the initial range of pH (pH < 3), the uptake of Fe^{2+} ions was weak: < 5% removal. However, by increasing the pH from 3 to 6 the uptake of iron (II) was strongly affected with the change in the medium pH: indeed Fe (II) adsorption increased significantly from 5% to about 90%. At the latter stage of pH, *i.e.* beyond pH~ 8.5, the iron (II) removal attained maximum percentages from ~97.3 up to ~99.4%.

In order to understand the pH dependence of Fe (II) adsorption, it is necessary to take into account the physicochemical surface properties of zeolitized brick as well as the chemical form(s) of iron(II) entities present at the brick-water interface.

The deposition of zeolite(s) crystals on the surface of the brick contributed to change the electro-kinetic properties of this material. The pH_{PZC} of alkaline brick samples was found to be in the pH range 5.83-5.89, which was somewhat higher than that of untreated brick: ~5.3. The surface of alkaline brick then carried positive charges below the pH range 5.83-5.89 and became negatively charged beyond these pH values. This explained why the removal percentage of iron(II) attained progressively maximum levels and a plateau beyond pH 6, as shown in Fig. 9.

On the other hand, from chemical Fe (II) speciation (Visual MINTEQ studies; see above) it was shown that, in the pH range 6.0-7.1 measured at the equilibrium state of the solid-liquid (batch) system, the free Fe^{2+} ion predominated in the liquid phase. Therefore, it was assumed

that electrostatic attraction forces should intervene between brick surfaces with negative charges and free Fe^{2+} ions, and thereby should cause metal uptake. It is worth noting that, in the pH range of performed batch experiments, the uptake of Fe^{2+} ions occurred in the plateau of the plot: Fe (II)-removal % *vs* pH shown in Fig. 9.

3.4.3 Na^+/Fe^{2+} exchange in batch reaction

In addition to electrostatic attraction, a surface complexation through an ion-exchange process was postulated for uptake of iron (II) in the pH region of performed batch experiments (see section 3.2.3). Among the numerous combinations of possible reaction stoichiometries, batch adsorption data were fitted reasonably by assuming the following chemical reaction:

$$2[>S{-}O^{-}(H_2O)_nNa)^{+}]_{(brick)} + [Fe(H_20)_6^{2+}]_{(solution)} \longrightarrow (>S{-}O)_2Fe_{(brick)} + 2[Na(H_2O)_6^{+}]_{(solution)} + (2n\text{-}6)H_2O \quad (18).$$

This reaction would assume that a bidendate complex, $(>S{-}O)_2Fe_{(brick)}$, was formed at the brick surface as the final product of Fe(II) adsorption.

In this assumption, it should be interesting to know if the existence of such a bidendate species generated through reaction (18) was consistent with NMR spectroscopic results.

3.4.4 ^{23}Na and ^{1}H MAS NMR study

When compared to the ^{23}Na MAS NMR spectrum of raw brick (see Fig. 10A(a)), under our experimental conditions the alkaline treatment of the brick produced a broad signal in the ^{23}Na MAS NMR spectrum with a maximum intensity peak at -4 ppm and a weaker peak at around -25 ppm (Fig. 10A(b)). The spectrum shape observed was comparable to that reported by Glid and his co-workers (2017) for alkaline activated metakaolinite samples [104]. The spectral broadening detected was in fact due to the presence of several ^{23}Na NMR resonances (not interpreted here) resulting from the binding of Na^+ ions with different types of reactive sites present in the structures of brick zeolites. It is important to note that the chemical shift of the broad ^{23}Na NMR signal was further close to that observed for hydrated sodium ions, indicating the presence of water molecules in the combinations/complexations of Na^+ ions with reactive sites of alkaline brick.

In the case of the ^{1}H MAS NMR spectrum of alkaline brick, it was observed a broad and intense resonance at around 4.8 ppm accompanied with weak and sharp peaks at 4.3 ppm and ~3.8 ppm (Fig. 10B(a)).

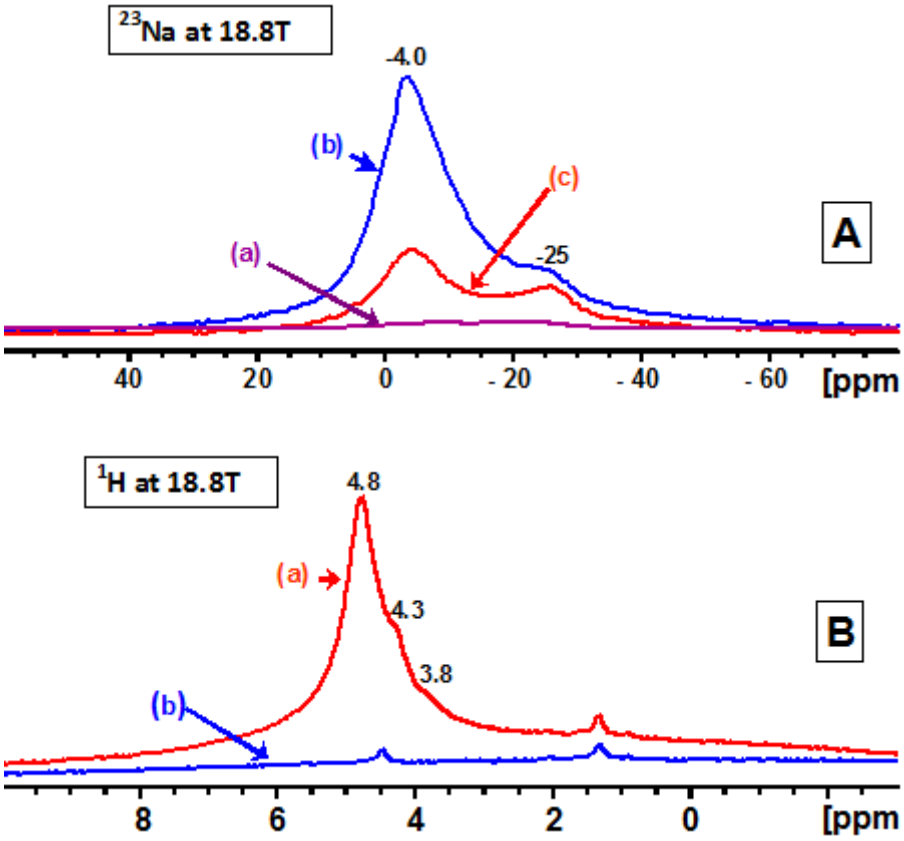

Figure 10: (A) ^{23}Na MAS NMR spectra of: (a) raw brick (a); (b) zeolitized brick; and (c) recovered zeolitized brick after iron(II) adsorption; (B) ^{1}H MAS NMR of zeolitized brick: (a) before; and (b) after iron(II) adsorption.

The appearance of a broad spectral spreading between ~2 ppm and ~8 ppm suggested that various water molecules and proton species were distributed in different atomic environments of the zeolitized-brick framework. And particularly, most of these ^{1}H NMR resonances were ascribed to water molecules associated distinctively with Na^{+} ions in the zeolitic frameworks, in agreement with previous NMR results on ^{23}Na atoms in the metakaolinite structure after its alkali activation [104]. Again, as observed for ^{23}Na atoms of alkaline brick, the chemical shift of this ^{1}H NMR resonance is close enough to that observed for Na^{+} ions in aqueous solutions ([105-108]. This finding confirmed two points: (i) sorbed Na^{+} ions are in a hydrated form, $Na(H_2O)_n^{+}$; and (ii) the binding of hydrated sodium with

negatively charged brick sites (>S–O^- with S = Si and Al) would result in outer-sphere complexes owing to electrostatic attraction forces ([108].

After Fe(II) adsorption, the ^{23}Na and ^{1}H MAS NMR of recovered brick samples changed significantly. Indeed, as shown in Fig. 10A(c) and 10B(b) the ^{23}Na and ^{1}H MAS NMR resonances relative to sodium and water hydrogen which were initially incorporated into the alkaline-brick framework, decreased dramatically, suggesting the release of Na^+ ions and water molecules from the alkaline brick.

4. CONCLUSION:

The zeolitization of a brick containing metakaolinite was performed in this work and ESEM/EDS analysis showed the formation of crystals of zeolites NaA and/or NaP deposited at the brick surface. The uptake of Fe^{2+} ions from aqueous solutions by zeolitized brick was afterward studied from batch experiments. The equilibrium data obtained were analyzed using Langmuir, Freundlich, and Dubinin-Radushkevich isotherms. Langmuir isotherm revealed the best fit, suggesting the involvement of monolayer coverage of Fe^{2+} ions on to brick surfaces. Dubinin-Radushkevich isotherm investigations showed that the adsorption of Fe^{2+} ions on zeolitized-brick surfaces referred to a chemisorption mechanism which is in agreement with conclusions made by applying the Freundlich isotherm model. Analysis of experimental (batch) data further revealed the existence of an ion-exchange between Fe^{2+} ions (in the liquid phase) and Na^+ ions at the brick-water interface according to an atomic Fe/Na ratio close to 1:2 (*i.e.* according to the stoichiometry: $1Fe^{2+}$:$2Na^+$). Thermodynamic parameters were calculated from distribution and partition coefficients, and the comparison of data showed no significant difference. Thermodynamic adsorption findings revealed that the process occurred spontaneously ($-\Delta G°$), in an endothermic nature ($+\Delta H°$), and with increased randomness ($+\Delta S°$).

As for NMR results, they revealed two relevant points: (i) an ion-exchange reaction between hydrated sodium (bound to brick surfaces) and Fe^{2+} ions (in the liquid phase) occurring at the brick-water interface, thus confirming batch data; and (ii) the absence (or weak implication) of water molecules in the association of iron(II) ions with reactive brick sites, in agreement with adsorption reaction (18).

ACKNOWLEDGMENT:

This research was partly funded by the "Agence de l'Eau Artois-Picardie," and the "City Hall of Villeneuve d'Ascq". These investigations were undertaken successfully owing to the cooperation between the University of Lille1 (France) and the University of Bangui (Central African Republic). This collaboration (being still underway) and the Grant-in-Aid to Ms. N. Poumaye in for her Doctoral-Thesis preparation have been financially supported by the Embassy of France to Bangui. The authors gratefully thank David Dumoulin (Chemical Engineer) and Christine Grare and V. Alaimo (Chemical Technicians) for helping us usefully in certain delicate chemical and/or analytical/spectroscopic analyses, and Laurence Burylo for having recorded and indexed X-ray diffractograms of our samples.

REFERENCES:

1. World Health Organization, Guidelines for Drinking Water Quality, recommendations, Vol. 1, WHO, Geneva, Switzerland, 1984, p. 79.
2. S. Chaturvedi, P.N. Dave, Removal of iron for safe drinking water, Desalination 303 (2012) 1-11.
3. N. Khatri, S. Tyagi, D. Rawtani, Recent Strategies for the removal of iron from water: A review, Journal of Water Process Engineering 19 (2017) 291-304.
4. G.D. Michalakos, J.M. Nieva, D.V. Vayenas, G. Lyberatos, Removal of iron from potable water using a Trickling filter, Wat. Res. 31 (5) (1997) 991–996.
5. P. Colvin, V. Filipova, A. Masic, Iron Removal.VVAN01 Decentralized Water and Wastewater Treatment, (2017) www.chemeng.lth.se/vvan01/Arkiv/ExerciseB_ Iron removal.pdf2011
6. Tech Brief: Iron and Manganese Removal, A National Drinking water Clearinghouse Fact Sheet, NINE-September 1998, item #DWBLPE70, 1998, pp. 1-4.
7. J. Hartmann, F. Braulke, U. Sinzig, G. Wulf, J.H. Maas, F. Konietschke, D. Haase, Iron overload impairs proliferation of erythroid progenitors cells (BFU-E) from patients with myelodysplastic syndromes, Leuk. Res. 37 (2013) 327–332.
8. X. Chai, D. Li, X. Cao, Y. Zhang, J. Mu, W. Lu, X. Xiao, C. Li, J. Meng, J. Chen, Q. Li, J. Wang, A. Meng, M. Zhao, ROS-mediated iron overload injuries the hematopoiesis of bone marrow by damaging hematopoietic stem/progenitor cells in mice, Sci. Rep. 5 (2015) 10181.
9. Y.Y. Jang, S.J. Sharkis, A low level of reactive oxygen species selects for primitive hematopoietic stem cells that may reside in the low-oxygenic niche, Blood 110 (2007) 3056–3063.
10. L. Shao, H. Li, S.K. Pazhanisamy, A. Meng, Y. Wang, D. Zhou, Reactive oxygen species and hematopoietic stem cell senescence, Int. J. Hematol. 94 (2011) 24–32.
11. C. Frippiat, J. Dewelle, J. Remacle, O. Toussaint, Signal transduction in H_2O_2 induced senescence-like phenotype in human diploid fibroblasts, Free Radic. Biol. Med. 33 (2002) 1334–1346.
12. E. Prus, E. Fibach, Effect of iron chelators on labile iron and oxidative status of thalassaemic erythroid cells, Acta Haematol. 123 (2010) 14–20.
13. D. Vries, C. Bertelkamp, F. Schoonenberg Kegel, B. Hofs, J. Dusseldorp, J.H. Bruins, W. de Vet, B. van den Akker, Iron and manganese removal: Recent advances in modeling treatment efficiency by rapid sand filtration, Water Research 109 (2017) 35-45.
14. S. Vigneswaran, C. Visvanathan, Water Treatment Processes: Simple Options, CRC Press, New York, NY, 1961, pp. 224.

15. D. A. white, A. As far-Siddique, Removal of manganese and iron from drinking water using hydrous manganese dioxide, Solvent Extraction and Ion Exchange 15 (6) (1997) 1133-1145. Published online: 16 May 2007. https://doi.org/10.1080/07366299708934526
16. W.R. Knocke, J.E. Van Benschoten, M.J. Kearney, A.W. Soborski, D.A. Reckhow, Kinetics of manganese and iron oxidation by potassium permanganate and chlorine dioxide, Journal - American Water Works Association 83 (6) (1991) 80-87.
17. R.B. Robinson, State-of-the-Art: Iron and Manganese Control, In Proceedings of the New England Water Works Association Conference and Exhibition. Marlborough, MA, 1998.
18. C. Lessard, D. Ellis, J. Serodes, C. Bouchard, Oxydation du fer et du manganese dans le traitement des eaux souterraines, Vecteur Environ. 32 (1999) 30-37.
19. D. Ellis, C. Bouchard, G. Lantagne, Removal of iron and manganese from groundwater by oxidation and microfiltration, Desalination 130 (2000) 255-264.
20. P. Phatai, J. Wittayakun, W.-H. Chen, C. M. Futalan, N. Grisdanurak, C.-C. Kan , Removal of manganese(II) and iron(II) from synthetic groundwater using potassium permanganate, Desalination and Water Treatment 52 (31-33) (2014) 5942-5951.
21. G. D.Michalakos, J. M. Nieva, D.V. Vayenas, G. Liberatos, Removal of iron from potable water using a trickling filter, Water Research 31 (5) (1997) 991-996.
22. A. G. Tekerlekopoulou, I.A. Vasiliadou, D.V. Vayenas, Physico-chemical and biological iron removal from potable water, Biochemical Engineering Journal 31 (2006) 74-83.
23. A. G. Tekerlekopoulou, D.V. Vayenas, Ammonia, iron and manganese removal from potable water using trickling filters, Desalination 210 (2007) 225-235.
24. S. Qin, F. Ma, P. Huang, J. Yang, Fe(II) and Mn(II) removal from drilled well water: A case study from a biological treatment unit in Harbin, Desalination 245 (2009) 183-193.
25. Mike Keller, Iron removal by ion exchange: Standing on the solid ground, water Cond. Purif. (June 2004) 20-23.
26. S.S. Madaeni, A.G. Fane, G.S. Grohmann, Virus removal from water and wastewater using membranes, J. Membr. Sci. 102 (1995) 65-75.
27. Y.J. Chang, K.H. Choo, M.M. Benjamin, S. Reiber, Combined adsorption/UF process increases TOC removal, J. Am. Water Works Assoc. 90 (5) (1998) 57-71.
28. S.J. Lee, K.H. Choo, C.H. Lee, Conjunctive use of ultrafiltration with powdered activated carbon adsorption for removal of synthetic and natural organic matter, J. Ind. Eng. Chem. 6 (2000) 357-361.
29. G.K. Pearce, M. Heijnen, J. Rockhouse, Using ultrafiltration membrane technology to meet UK Cryptosporidium regulations, Membr. Technol. 1 (2002) 6-9.
30. K.W. Lee, K.H. Choo, S.J. Choi, K. Yamamoto, Development of an integrated iron oxide adsorption/membrane separation system for water treatment, Water Sci. Technol. Water Supply 2 (2002) 293-300.
31. K.H. Choo, H. Lee, S.J. Choi, Iron, and manganese removal and membrane fouling during UF in conjunction with prechlorination for drinking water treatment, J. Membr. Sci. 267 (2005) 18-26.
32. M. Pettinato, S. Chakraborty,n, Hassan A. Arafat, V. Calabro, Eggshell: A green adsorbent for heavy metal removal in an MBR system, Ecotoxicology and Environmental Safety 121 (2015) 57–62.
33. X Du, Guangyang Liu, Fangshu Qu, Kai Li, Senlin Shao, Guibai Li, Heng Liang, Removal of iron, manganese, and ammonia from groundwater using a PAC-MBR system: The anti-pollution ability, microbial population, and membrane fouling, Desalination 403 (2017) 97–106.
34. R.B. Meagher, Phytoremediation of toxic elemental and organic pollutants, Curr. Opin. Plant Biol. 3 (2) (2000) 153-162.
35. P. Berbenni, A. Pollice, R. Canziani, L. Stabile, F. Nobili, Removal of iron and manganese from hydrocarbon-contaminated groundwaters, Bioresour. Technol., 74 (2000) 109-114.
36. D.R. Lovley, Cleaning up with genomics: Applying molecular biology to bioremediation, Nat. Rev. Microbiol. 1 (1) (2003) 35-44.
37. A.I. Zouboulis, I.A. Katsoyiannis, Recent advances in the bioremediation of arsenic-contaminated groundwaters, Environ. Int. 31 (2005) 213-219.

38. E. Diaz (Ed.), In Microbiol biodegradation: Genomics and Molecular biology, 1st ed., Caister Academic Press ISBN, 1904455174, 2008.
39. W.C. Andersen, T.J. Bruno, Application of gas-liquid entraining rotor to supercritical fluid extraction: removal of iron(III) from water, Anal. Chim. Acta 485 (2003) 1-8.
40. N.A. Yavorovsky, S.S. Peltsman, J.I. Kornev, Yu, V. Volkov, Technology of Water Treatment Using Pulsed Electric Discharges, In Proceedings of the 4th Korea-Russia International Symposium on Science and Technology, Ulsan, Korea, Vol. 3 (2000) 422-427.
41. M.A. Malik, A. Ghaffar, S.A. Malik, Water purification by electric discharges, Plasma Sources Sci. Technol., Vol. 10, No 1, 2001, 82-91.
42. G. Chen, Electrochemical technologies in wastewater treatment, Separation and Purification Technology 38 (2004) 11–41.
43. J.P. Duguet, A. Bruchet, J. Mallevialle, New Advances in Oxidation Processes: The use of Ozone/hydrogen Peroxide Combination for Micropollutant Removal in Drinking Water, Water Supply 7 (4) (1989) 115-124.
44. J. W. Kang, H.S. Park, R.Y. Wang, M. Koga, K. Kadokami, H.Y. Kim, E.T. Lee, S.M. Oh, Effect of Ozonation for treatment of micropollutants present in a drinking water source, water Science and Technology 36 (12) (1997) 299-307.
45. L.V. Serikov, E.A. Tropina, L.N. Shiyan, F.H. Frimmel, G. Metreveli, M. Delay, Iron oxidation in different types of groundwater of Western Siberia, Journal of Soils and Sediments 9 (2) (2009) 103-110.
46. C. Gottschalk, J.A. Libra, A. Saupe, Ozonation of Drinking Water and of Wastewater: A Practical Guide to Understanding Ozone and its Application. Wiley, Weinheim, 2010.
47. T. Juhna, E. Melin, Ozonation and Biofiltration in Water Treatment- Operational Status and Optimization Issues, TECHNEAU, D.5.3.1.B, December 2006, pp. 1-79.
48. B. Das, P. Hazarika, G. Saikia, H. Kalita, D.C. Goswami, H.B. Das, S.N. Dube, R.K. Dutta, Removal of iron from groundwater by ash: A systematic study of a traditional method, J. Hazard. Mater. 141 (2007) 834-841.
49. P. Maneechakr, S. Karnjanakom Adsorption behavior of Fe(II) and Cr(VI) on activated carbon: Surface chemistry, isotherm, kinetic and thermodynamic studies. J. Chem. Thermodynamics 106 (2017) 104-112.
50. A.R. Kaveeshwar, S.K. Ponnusamy, E.D. Revellame, D.D. Gang, M.E. Zappi, R. Subramaniam, Pecan shell based activated carbon for removal of iron(II) from fracking wastewater: Adsorption kinetics, isotherm and thermodynamic studies, Process Safety and Environmental Protection 114 (2018) 107-122.
51. G.M. Walker, G. Connor, S.J. Allen, Kinetics of iron(II) removal from aqueous solution using activated dolomite, Open Chem. Eng. J. 1 (2007) 23-29.
52. K.G. Bhattacharyya, S.S. Gupta, Adsorption of a few heavy metals on natural and modified kaolinite and montmorillonite: A Review, Adv. Colloid Interface Sci. 140 (2008) 114-131.
53. K.G. Bhattacharyya, S.S. Gupta, Kaolinite and montmorillonite as adsorbents for Fe(III), Co(II) and Ni(II) in an aqueous medium, Applied Clay Science 41(1) (2008) 1-9.
54. D. Qin, X. Niu, M. Qiao, G. Liu, H. Li, Z. Meng, Adsorption of ferrous ions onto montmorillonites, Applied Surface Science 333 (2015) 170-177.
55. JS. Kim, M.A. Keane, The removal of iron and cobalt from aqueous solutions by ion exchange with Na-Y zeolite: batch, semi-batch, and continuous operation, J. Chem. Technol. Biotechnol. 77 (2002) 633-640.
56. A.S. Sheta, A.M. Falatah, M.S. Al-Sewailem, E.M. Khalid, A.S.H. Sallam, Sorption characteristics of zinc and iron by natural zeolite and bentonite, Microporous and Mesoporous Mater. 61 (2003) 127-136.
57. M.K. Doula, Removal of Mn^{2+} ions from drinking water by using clinoptilolite-Fe oxide system, Water Research 40 (2006) 3167-3176.
58. A.M. Anielak, M. Arendacz, Iron and manganese removal effects using zeolites, Ochrona Srodowiska 9 (2007) 9-18.
59. M. Al-Anber, Z.A. Al-Anber, Utilization of natural zeolite as ion-exchange and sorbent material in the removal of iron, Desalination 255 (2008) 70-81.
60. D. Barlokova, J. Ilavsky, Removal of iron and manganese from water using filtration by natural materials, Polish Journal of Environmental Studies 19 (6) (2010) 1117-1122.

61. R. P. Azar, C. Falamaki, Removal of aqueous Fe^{2+} using MnO_2-clinoptilolite in a batch slurry reactor: Catalyst synthesis, characterization and modelling of catalytic behaviour, Journal of Industrial and Engineering Chemistry 18 (2012) 737-743.
62. O. Nazarenko, R. Zarubina, Application of Sakhaptinsk zeolite for improving the quality of groundwater, Energy and Environmental Engineering 1 (2) (2013) 68-73.
63. M.K. Seliem, S. Kormarneni, Equilibrium and kinetic studies for dissociation of iron from aqueous solution by synthetic Na-A zeolites: Statistical modelling and optimization 228 (2016) 266-274.
64. S. Cinar, B. Beler-Baykal, Ion exchange with natural zeolites: an alternative for water softening? Water Science et Technology 51 (2005) 71-77.
65. L. Lazar, B. Bandrabur, R.-E. Tataru-Farmus, M. Drobota, S.-G. Stroe, G. Gutt, Equilibrium performances of *CRYSTAL-RIGHT™ CR100* zeolite used in water softening process. Environmental Engineering and Management Journal, 14(3) (2015) 541-549.
66. D.W. Breck, Zeolite Molecular Sieves Structure, Chemistry, and Use. John Wiley & Sons, New York, 1974.
67. L.B. Sand, F.A. Mumpton, Natural Zeolites: Occurrence, Properties, Use. Oxford; New York: Pergamon Press, 1978, pp. 546.
68. S.C. Dehou, M. Wartel, P. Recourt, B. Revel, J. Mabingui, A. Montiel, A. Boughriet, Physicochemical, crystalline and morphological characteristics of bricks used for ground waters purification in Bangui region (Central African Republic). Applied Clay Science, 59-60 (2012) 69-75.
69. M.M.J. Treacy, J.B. Higgins, Collection of Simulated XRD Powder Patterns for Zeolites (4th Revised Edition), Elsevier, New York, 2001, pp. 174-175 and 212-215.
70. S. Tontisirin, Synthesis and characterization of co-crystalline zeolite composite of LSX/A. Microporous and Mesoporous Materials 239 (2017) 123-129.
71. M. Sathupunya, E. Glari, S. Wongkasemjit, ANA and GIS zeolite synthesis directly from alumatrane and silatrane by sol-gel process and microwave technique. J.EUR. Ceram. Soc. 22 (2002) 2305-2314.
72. H.-L. Zubowa, H. Kosslick, D. Müller, M. Richter, L. Wilde, R. Fricke, Crystallization of phase-pure zeolite NaP from MCM-22-type gel compositions under microwave radiation. Microporous and Mesoporous Materials 109 (2008) 542–548.
73. S. Khabuanchalad, P. Khemthong, S. Prayoonpokarach, J. Wittayakun, Transformation of zeolite NaY synthesized from rice husk silica to NaP during hydrothermal synthesis. Suranaree J. Sc. Technol. 15 (2008) 225-231.
74. J. Behin, H. Kazemian, S. Rohani, Sonochemical synthesis of zeolite NaP from clinoptilolite. Ultrasonics Sonochemistry 28 (2016) 400-408.
75. I. Langmuir, The constitution and fundamental properties of solids and liquids. PART I. Solids. J. Am. Chem. Soc. 38 (1916) 2221-2295.
76. I. Langmuir, The adsorption of gases on plane surfaces of glass, mica and platinum, J. Am. Chem. Soc. 40 (1918) 1361–1403.
77. K.R. Hall, L.C. Eagleton, A. Acrivos, T. Vermeulen, Pore- and solid-diffusion kinetics in fixed-bed adsorption under constant-pattern conditions, Ind. Eng. Chem. Fundam. 5 (1966) 212–223.
78. T.W. Weber, R.K. Chakravorti, Pore and solid diffusion models for fixed-bed adsorbers. AICHE J. 20 (1974) 228-238.
79. H. Freundlich, Über die adsorption in Lösungen, Zeitschrift für Physikalische Chemie 57 (1906) 385–471.
80. M. Matouq, N. Jildeh, M. Qtaishat, M. Hindiyeh,M.Q. Al Syouf, The adsorption kinetics and modelling for heavy metals removal from wastewater by Moringa pods. J. Environ.Chem. Eng. 3 (2) (2015) 775-784.
81. M.M. Dubinin, E.D. Zaverina, L.V. Radushkevich, Sorption and structure of active carbons, I. Adsorption of organic vapors. Zh. Fiz Khim. 21 (1947) 1351-1362.
82. O. Ceylan, D. Baybas, Adsorption of some textile dyes by hexadecyltrimethylammonium bentonite, Turk. J. Chem. 25 (2001) 193-200.
83. Y. S. Ho, J. F. Porter, G. McKay, Equilibrium isotherm studies for the sorption of divalent metal ions onto peat: Copper, nickel and lead single component systems, Water, Air, and Soil Pollution 141 (1-4) (2002) 1–33.
84. T. S. Singh, K.K. Pant, Equilibrium, kinetics and thermodynamic studies for adsorption of As(III) on activated alumina, Separation and Purification Technology (2004) 139-147.

85. S. Rengaraj, Y. Kim, C.K. Joo, K. Choi, J. Yi, Batch adsorptive removal of copper ions in aqueous solutions by ion exchange resins: 1200H and IRN97H, Korean Journal of Chemical Engineering 21 (1) (2004) 187–194.
86. E. Erdem, N. Karapinar, R. Donat, The removal of heavy metal cations by natural zeolites, Journal of Colloid and Interface Science 280 (2004) 309–314.
87. V.J. Inglezakis, Solubility-normalized Dubinin–Astakhov adsorption isotherm for ion-exchange systems, Microporous and Mesoporous Materials 103 (2007) 72–81.
88. F.G. Helfferich, Ion Exchange, McGraw-Hill, New York (1962) pp. 624.
89. W. Rieman, H.F. Walton, Ion Exchange in Analytical Chemistry, in: International Series of Monographs in Analytical Chemistry, Vol. 38, Pergamon, Oxford (1970) pp. 295.
90. K.Y. Foo, B.H. Hameed, Insights into the modelling of adsorption isotherm systems, Chem. Eng. J. 156 (2010) 2-10.
91. E. Wibowo, M. Rokhmat, Sutisna, Khairurrijal, M. Abdullah, Reduction of seawater salinity (Clinoptilolite): Adsorption isotherms, thermodynamics and kinetics, Desalination 409 (2017) 146-156.
92. A.A. Khan, R.P. Singh, Adsorption thermodynamics of carbofuran on Sn(IV) arsenosilicate in H^+, Na^+ and Ca^{2+} forms, Colloids Surf. 24 (1) (1987) 33-42.
93. M. Al-Ghouti, M.A.M. Khraisheh, M.N.M. Ahmad, S. Allen, Thermodynamic behavior and the effect of temperature on the removal of dyes from aqueous solution using modified diatomite: a kinetic study, J. Colloid Interface Sci. 287 (2005) 6–13.
94. S. Yang, L. Li, Z. Pei, C. Li, J. Lv, J. Xie, B. Wen, S. Zhang, Adsorption kinetics, isotherms and thermodynamics of Cr(III) on graphene oxide, Colloids and Surfaces A: Physicochem. Eng. Aspects 457 (2014) 100–106.
95. A.A. Taha, M. A. Shreadah, A.M. Ahmed, Hany Fathy Heiba, Multi-component adsorption of Pb(II), Cd(II), and Ni(II) onto Egyptian Na-activated bentonite; equilibrium, kinetics, thermodynamics, and application for seawater desalination, Journal of Environmental Chemical Engineering Journal of Environmental Chemical Engineering 4 (2016) 1166–1180.
96. C.S. Patrickios, E.N. Yamasaki, A correction to the calculation of the Gibbs free energy of adsorption for biomolecules in ion-exchange systems, Biophys. Chem. 69 (2-3) (1997) 219-220.
97. S.K. Milonjic, A consideration of the correct calculation of the thermodynamic parameters of adsorption, J. Serb. Chem. Soc. 72 (12) (2007) 1363-1367.
98. S. Canzano, Comment on: Removal of anionic dye Congo red from aqueous solution by raw pine and acid-treated pine cone powder as adsorbent: equilibrium, thermodynamic, kinetics, mechanism and process design, Water Res. 46 (13) (2012) 4314-4315.
99. S.K. Milonjic, Comments on removal of uranium(VI) from aqueous solution by adsorption of hematite, by X. Shuibo, Z. Chun, Z. Xinghuo, Y. Jing, Z. Xiaojian, W. Jingsong, J. Environ. Radioact. 100 (10) (2009) 921-922.
100. H.N. Tran, S.-J. You, H.-P. Chao, Thermodynamic parameters of cadmium adsorption onto orange peel calculated from various methods: A comparison study, J. Environ. Chem. Eng. 4 (2016) 2671-2682.
101. T. Sheela, Y.A. Nayaka, R. Viswanatha, S. Basavanna, T.G. Venkatesha, Kinetics and thermodynamics studies on the adsorption of Zn(II), Cd(II) and Hg(II) from aqueous solution using zinc oxide nanoparticles, Powder Technol. 217 (2012) 163-170.
102. X. Zhang, C. Jiao, J. Wang, Q. Liu, R. Li, P. Yang, M. Zhang, Removal of uranium(IV) from aqueous solutions by magnetic Schiff base: kinetic and thermodynamic investigation, Chem. Eng. J. 198-199 (2012) 412-419.
103. J.W. Morse, F.T. Mackenzie, Geochemistry of Sedimentary Carbonates, Elsevier Sci. Publishers B.V. (1990) pp. 707.
104. M. Glid, I. Sobrados, H. Ben Rhaiem, J. Sanz, A. Ben Haj Amara, Alkaline activation of metakaolinite-silica mixtures: Role of dissolved silica concentration on the formation of geopolymers. Ceramics International 43 (2017) 12641-12650.
105. H. Ohtaki, T. Radnai, Structure and dynamics of hydrated ions. Chem. Rev. 93 (1993) 1157-1204.
106. X. Xue, J.F. Stebbins, ^{23}Na NMR chemical shifts and local sodium coordination environments in silicates crystals, melts, and glasses. Phys. Chem. Mineral. 20 (1993) 297-307.

107. J.J. Jacobsen, N.C. Nielsen, H. Lindgreen, Sequences of charged sheets in rectorite. Am. Mineral. 80 (1995) 247-252.
108. Y. Kim, R.J. Kirkpatrick, ^{23}Na and ^{133}Cs NMR study of cation adsorption on mineral surfaces: local environments, dynamics, and effects of mixed cations. Geochim. Cosmochim. Acta 61(24) (1997) 5199-5208.